Clean wurtzite InN surfaces prepared with atomic hydrogen

L. F. J. Piper, T. D. Veal, M. Walker, I. Mahboob, and C. F. McConville[a)]
Department of Physics, University of Warwick, Coventry, CV4 7AL, United Kingdom

Hai Lu and W. J. Schaff
Department of Electrical and Computer Engineering, Cornell University, Ithaca, New York 14853

(Received 29 November 2004; accepted 4 April 2005; published 7 June 2005)

Conventional methods of surface preparation for III–V semiconductors, such as thermal annealing and sputtering, are severely limited for InN, resulting in In-enrichment and the introduction of donorlike defects. This is explained in terms of the unusually low Γ-point conduction band minimum of InN with respect to its Fermi stabilization energy. Here, low energy atomic hydrogen irradiation is used to produce clean wurtzite InN surfaces without such detrimental effects. A combination of x-ray photoelectron spectroscopy (XPS) and high-resolution electron-energy-loss spectroscopy was used to confirm the removal of atmospheric contaminants. Low energy electron diffraction revealed a (1×1) surface reconstruction after cleaning. Finally, XPS revealed In/N intensity ratios consistent with a predominantly In polarity InN film terminated by In-adlayers in analogy with *c*-plane GaN{0001}-(1×1) surfaces. © *2005 American Vacuum Society.*
[DOI: 10.1116/1.1927108]

The preparation of clean, well-ordered, and stoichiometric surfaces of III–V semiconductors is crucial for studying their surface and near-surface properties. Ideally, surface characterization is undertaken in a vacuum chamber connected to the epitaxial growth facility. However, when such facilities are unavailable, various *in situ* preparation methods, such as high temperature annealing and low energy ion bombardment and annealing (IBA), are routinely used. Preparation of clean InN surfaces using these techniques is difficult for two reasons. The first is the fact that the oxide desorption temperature exceeds the low dissociation temperature of InN.[1] As a result, cleaning by annealing is restricted to low temperatures in order to prevent In-enrichment, and is therefore largely ineffective. The second reason is associated with the unusually low conduction band minimum (CBM) at the Γ-point of InN.[2] The location of the Γ-point CBM, below the Fermi stabilization energy, favors the existence of donor impurities and formation of donorlike defects.[3] A similar situation exists for InAs.[4] The standard method of *in situ* cleaning of III–V surfaces, using cycles of low energy IBA, has been shown to result in severe structural damage and the introduction of donorlike defects for InAs surfaces.[5] Therefore, IBA is also unsuitable for InN. Indeed, recent studies of InN surface preparation have shown that Ar^+ IBA results in In-enrichment due to preferential sputtering.[6] Whilst this effect can be minimized by optimized sputtering conditions (grazing incidence and low ion energy) it cannot be completely eradicated. Further investigation of the electronic effects of IBA on InN surfaces is required.

In this article, the use of low energy (typically <1 eV) atomic hydrogen irradiation to produce clean InN surfaces is reported. A whole host of III–V surfaces have previously been successfully prepared by atomic hydrogen cleaning (AHC).[1] During AHC, surface oxides and other contaminants are removed by chemical reaction and subsequent desorption of the reaction products. The main advantage of this process lies in the fact that a significantly lower annealing temperature is required to remove the surface contaminants, although the exact H^* dosage and annealing temperature varies slightly depending on material. For InN, as mentioned previously, this fact is especially important to ensure clean, well-ordered, atomically flat, stoichiometric InN surfaces with limited N desorption.

An earlier attempt to clean InN surfaces by AHC was undertaken by Ohashi *et al.*[1] In their work they produced promising results, which indicated that H^* irradiation is effective in reducing native oxides using a thermal cracker with a $H_2\rightarrow H^*$ conversion efficiency of $\sim1.5\%$. In this work, clean, well-ordered, stoichiometric InN surfaces have been prepared using AHC. This was confirmed by a combination of x-ray photoelectron spectroscopy (XPS), low electron energy diffraction (LEED), and high-resolution electron-energy-loss spectroscopy (HREELS).

The InN layer investigated was unintentionally *n*-type doped. Details of the molecular beam epitaxial growth can be found elsewhere.[7] Single field Hall measurement indicated an average conduction electron density, *n*, of 1.83×10^{18} cm^{-3} and an average mobility of 1200 cm^2 V^{-1} s^{-1}. The polarity of the InN film was determined by coaxial impact collision ion scattering spectroscopy to be approximately 75% In-polarity and 25% N-polarity at the surface.[8]

The XPS spectra were recorded in an ultrahigh vacuum (UHV) chamber using a dual anode Mg K_α x-ray source (Vacuum Generators, UK) with a 100 mm concentric hemispherical electron energy analyzer (VSW, UK). A range of take-off angles (TOA) referenced to the surface of the sample, from 90° to 15°, were used. All of the binding energies were calibrated with respect to the adventitious hydrocarbon C 1*s* peak at 284.6 eV.[9] The HREEL spectra were obtained in a separate UHV chamber. The HREEL spectrom-

a)Electronic mail: c.f.mcconville@warwick.ac.uk

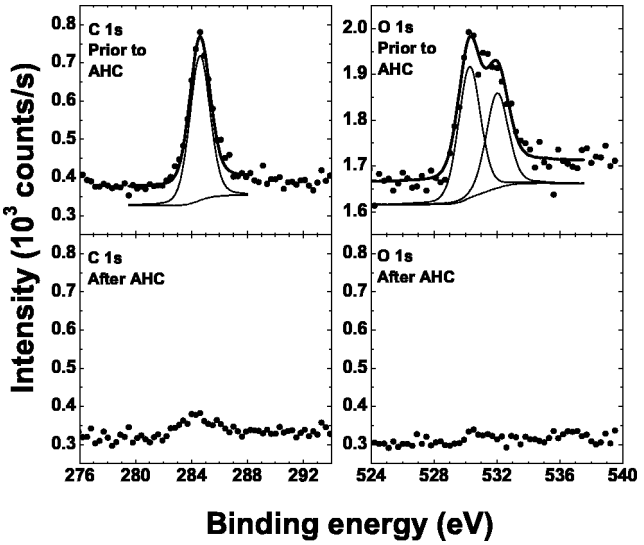

FIG. 1. The 45° TOA C 1*s* and O 1*s* core-level spectra (circles) recorded prior to and after AHC. For the prior to AHC spectra, for both the C 1*s* and O 1*s*, the corresponding fits (thick lines) are shown. The decomposed background and peak contributions of each fit (thin lines) are also shown vertically offset for all spectra.

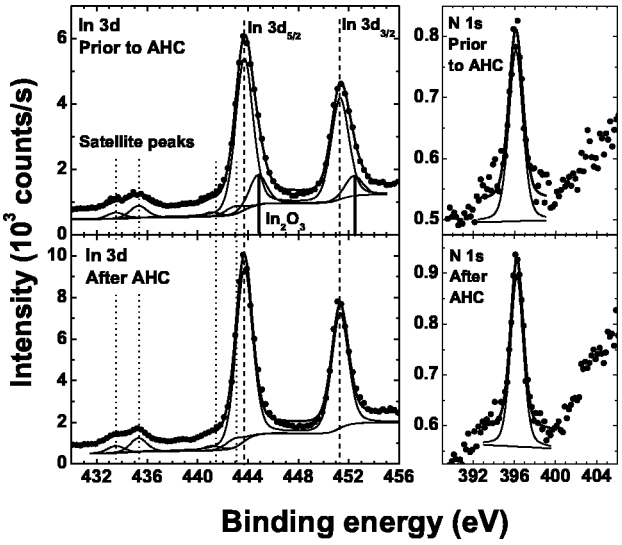

FIG. 2. The 45° TOA In 3*d* and N 1*s* core-level spectra (circles) recorded prior to and after AHC. For each spectrum the corresponding curve fit is also shown (thick lines). The decomposition of each fit into their background and peak components (thin lines) is also shown vertically offset for all spectra. Also highlighted in the In 3*d* spectra is the the spin–orbit In_2O_3 (solid lines) and In 3*d* (dashed lines) doublets and their corresponding satellite peaks (dotted lines). After AHC the spin–orbit In_2O_3 doublet is absent.

eter (VSW Ltd., UK) consists of a fixed monochromator and rotatable analyzer; both were of the 180° hemispherical deflector-type, with a four-element entrance- and exit-lens system. The instrumental resolution was typically 12 meV full width at half maximum (FWHM) in the elastic peak. The HREELS experiments were performed using a specular scattering geometry with an incident and scattered polar angle of 45°. Finally, both chambers were equipped with a retractable LEED optics (Omicron, Germany).

An Oxford Applied Research thermal gas cracker, with a cracking efficiency of ~50% was used to prepare the InN surface. In both UHV chambers the atomic hydrogen clean consisted of a 8 kL (1 kL = 10^{-3} Torr s) dose of hydrogen, followed by a further 8 kL at 450 K. Afterwards it was annealed at 575 K for 2 h before being left to cool to room temperature.

The 45° TOA core-level spectra of the C 1*s* and O 1*s* photoelectrons prior to and after AHC are shown in Fig. 1. It can be seen that prior to the clean, both the C 1*s* and O 1*s* spectra show strong signals. The x-ray photoemission spectra were curve fitted using a Shirley background and decomposing the core-level signals into Voigt line shapes (25% Lorentzian and 75% Gaussian) of equal FWHM (1.6 eV). A single peak at 284.6 eV describes the C 1*s* signal. For the prior to AHC O 1*s* spectra, two peaks are necessary to reproduce the data, with a more intense peak at 530.3 eV and a slightly less intense peak at 532.0 eV. The former is assigned to the In_2O_3 contribution, and the latter is assigned to adventitious oxygen. After AHC, both the C 1*s* and O 1*s* signals in Fig. 1 reduce to the background noise level. Although there is an indication that a C 1*s* peak remains after cleaning, it will be mentioned later that AHC is able to produce surfaces with contamination levels <0.1% of a monolayer.

In Fig. 2, the corresponding 45° TOA In 3*d* and N 1*s* core-level spectra prior to and after AHC are shown. The x-ray photoemission spectra are also curve-fitted using the same method as previously described for the C 1*s* and O 1*s* spectra. Before and after AHC, the N 1*s* spectrum is fitted by a single peak at 397.0 eV corresponding to the In–N bond.[10] The intensity at high binding energies (>400 eV) in the N 1*s* spectra in Fig. 2 is due to the shoulder from the Ta $4d_{5/2}$ peak at ~406 eV,[9] resulting from the Ta foil clips used to mount the sample. There is the possibility that the small C 1*s* peak after AHC may be associated with adventitious carbon from the Ta foil clips.

The spin–orbit doublet (7.6 eV) of the prior to AHC In 3*d* spectrum in Fig. 2 consists of two components, in contrast to the N 1*s* spectrum. The first In $3d_{5/2}$ component is located at 443.7 eV, corresponding to the In–N bond. The second In $3d_{5/2}$ component shifted by ~1 eV at 444.7 eV in Fig. 2 is attributed to the In_2O_3 bond.[9] Other features are due to the α_3 and α_4 satellite energies of the spin–orbit In 3*d* and In_2O_3 doublets from the Mg K_α source.[9] The In_2O_3 contributions to the spin–orbit In 3*d* doublet are absent after AHC, as shown in Fig. 2. The In/N ratio is determined from the In $3d_{5/2}$ and N 1*s* Voigt line shapes in the after the AHC spectra in Fig. 2 with the appropriate atomic sensitivity factors, yielding a ratio of In/N = 2.8 ± 0.7. Finally, LEED revealed a (1×1) surface reconstruction after cleaning, which is shown in the inset of Fig. 4.

The angular dependence of the In/N intensity ratio is plotted in the inset of Fig. 3. Also shown in Fig. 3 is the In 3*d* and N 1*s* core-level spectra after cleaning, at both 90° and 30° TOA. By decreasing the angle, the escape depth of the photoelectrons is reduced. As a result, the smallest TOA

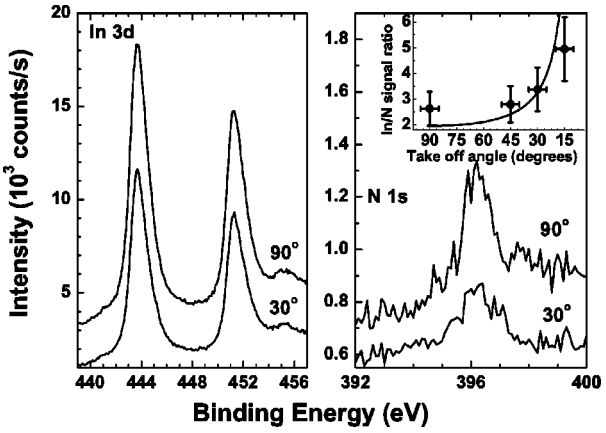

FIG. 3. The In 3*d* and N 1*s* core-level spectra after AHC, at both 90° and 30° TOA. The In/N intensity ratio determined from XPS against the angle is plotted in the inset. Also included in the inset is the calculated variation in the In/N photoelectron intensity ratio with angle, assuming an In-adlayer model analogous to GaN{0001}-(1×1) surfaces.

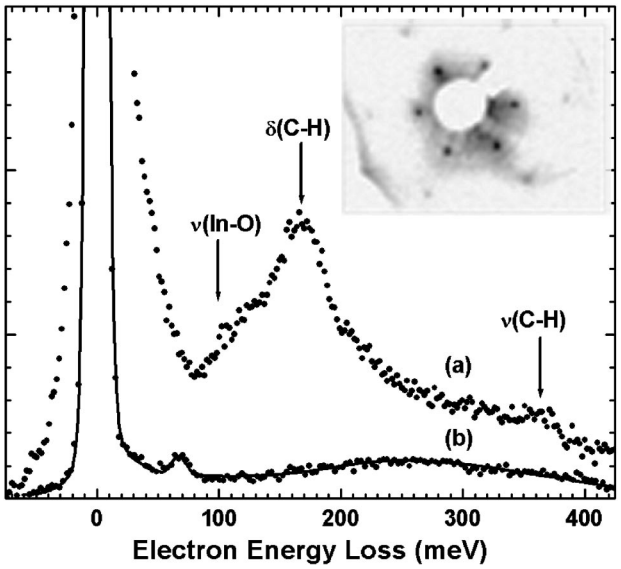

FIG. 4. The HREEL spectra (points) for a probing energy of 15 eV are shown (a) prior to and (b) after AHC. Surface contaminant vibrational modes are present in (a), whilst these contaminant modes are absent after AHC (b). The clean surface spectrum in (b) is simulated by semiclassical dielectric theory (line). The inset shows the (1×1) LEED pattern recorded after cleaning, using an electron energy of 164 eV.

spectra have the greatest surface sensitivity. By reducing the effective probing depth the counts are reduced, as seen in both the In 3*d* and N 1*s* spectra. However, the N 1*s* intensity is found to decrease by a greater amount relative to the In 3*d* signal. This is highlighted further in the inset of Fig. 3, with the increase in the In/N ratio with decreasing angle. Therefore, the surface region is found to be In-rich.

In order to further interpret the variation in the In/N intensity ratio with angle, model computations were performed by summing the In and N intensity contributions from each atomic layer, using the standard expression $I = I_0 \exp(-d/\lambda \sin\theta)$, where, I is the attenuated XPS intensity from an atomic layer of depth, d, for a TOA, θ. I_0 refers to the intensity from the layer if unattenuated and λ is the inelastic mean free path of the photoelectrons within the sample. Mean free path lengths of 12.28 Å for the In $3d_{5/2}$ photoelectrons and 11.41 Å for the N 1*s* photoelectrons are used in the modelling.[11] For a bulk-truncated In-terminated, In-polarity, stoichiometric wurtzite crystal, the expected In/N ratio is 1.1 at 45°. This is significantly smaller than the experimental ratio of $\mathrm{In/N} = 2.8 \pm 0.7$. However, comparisons with GaN provide a better interpretation of the In/N ratio. In-rich conditions are used during growth in order to achieve high quality InN,[12] suggesting that the InN surfaces are stabilized by In atoms by analogy with GaN grown under Ga-rich conditions.[13] It is believed that this behavior in GaN results from the large size difference between Ga and N, resulting in naturally occurring Ga-rich surface reconstructions.[13] A similar situation should also occur for InN but to a larger degree, because of the larger size mismatch between In and N. Auger electron spectroscopy measurements on GaN have revealed a 2–3 monolayer (ML) Ga-adlayer for Ga-polarity (0001) "pseudo" (1×1) surfaces and a 1 ML Ga-adlayer for N-polarity $(000\bar{1})$-(1×1) surfaces.[13] For Ga-polarity, a laterally contracted (1×1) Ga-bilayer has been calculated from first principles for GaN(0001).[14] It is reasonable to assume that a similar termination is one of the energetically favorable (1×1) reconstructions that can naturally exist at InN surfaces. Considering a similar adlayer situation for 75% In-polarity and 25% N-polarity, In-terminated, bulk stoichiometric, wurtzite InN, the In/N intensity ratio was calculated and is plotted in the inset of Fig. 3. It is in agreement with In/N intensity ratio determined by XPS, within error limits.

HREELS provides further indication that AHC produces clean, well-ordered InN surfaces. In HREELS, a monoenergetic beam of electrons impinges on the sample's surface and the scattered electrons are energy analyzed. The majority of the probing electrons are elastically scattered, giving rise to a peak at zero loss energy. The technique is especially sensitive to adsorbate vibrational modes associated with surface contaminants (to 0.1% of a monolayer[15]), which interact with the probing electrons. Other energy-loss features in the spectra are associated with the energy exchange between the incident electrons and the collective excitations of both the conduction electrons (plasmons) and the lattice (phonons).

The HREEL spectrum recorded prior to AHC in Fig. 4(a) shows several strong vibrational modes associated with atmospheric contaminants. These were confirmed as adsorbate vibrational modes since their peak intensity decreased as the probing energy, E, increased by the factor $E^{-1/2}$. The band between 80 and 120 meV is attributed to oxide vibrational modes, in this case the stretching mode $\nu(\mathrm{In-O})$.[5] The peaks at ~170 meV and ~360 meV are associated with the hydrocarbon deformation mode $\delta(\mathrm{C-H})$ and the hydrocarbon stretching mode $\nu(\mathrm{C-H})$, respectively.[5] After AHC, the FWHM of the elastic peak is reduced from 39 meV to 12 meV, as seen in Fig. 4(b). This FWHM of 12 meV is consistent the nominal spectrometer resolution for

the settings used. The adsorbate vibrational modes are no longer present in Fig. 4(b) indicating, as previously mentioned, that AHC produces contaminant free surfaces. The removal of the vibrational modes results in the appearance of the Fuchs–Kliewer phonon peak at ~66 meV and a conduction electron plasmon peak at ~250 meV, consistent with previous studies on clean InN surfaces.[2,16,17] The clean surface HREEL spectrum in Fig. 4(b) was simulated using semiclassical dielectric theory, details of which can be found elsewhere.[2] The simulation considers only the interaction between the probing electrons and the excitations arising from the conduction electrons and lattice vibrations. Only HREEL spectra from clean well-ordered InN surfaces can be successfully simulated.

It has been shown that an AHC process is able to overcome the problems associated with the low dissociation temperature and unusually low Γ-point CBM, to prepare clean, well-ordered surfaces of bulk stoichiometric InN. This was confirmed by a combination of XPS, HREELS, and LEED. Analysis of the XPS revealed angle dependent In/N intensity ratios consistent with initial calculations of mixed polarity InN with In-adlayers. The removal of atmospheric contaminant vibrational modes in the HREEL spectra further verified a clean and well-ordered InN surface.

[1]T. Ohashi, Y. Saito, T. Maruyama, and Y. Nanishi, J. Cryst. Growth **237–239**, 1022 (2002).
[2]I. Mahboob, T. D. Veal, L. F. J. Piper, C. F. McConville, H. Lu, W. J. Schaff, J. Furthmüller, and F. Bechstedt, Phys. Rev. B **69**, 201307(R) (2004).
[3]J. Wu and W. Walukiewicz, Superlattices Microstruct. **34**, 63 (2003).
[4]W. Walukiewicz, Phys. Rev. B **37**, 4760 (1988).
[5]G. R. Bell, C. F. McConville, and T. S. Jones, Appl. Surf. Sci. **104/105**, 17 (1996).
[6]S. Krischok, Y. Yanev, O. Balykov, M. Himmerlich, J. A. Schaefer, R. Kosiba, G. Ecke, I. Cimalla, V. Cimalla, O. Ambacher *et al.*, Surf. Sci. **566–568**, 849 (2004).
[7]H. Lu, W. J. Schaff, J. Hwang, H. Wu, W. Yeo, A. Pharkya, and L. F. Eastman, Appl. Phys. Lett. **77**, 2548 (2000).
[8]M. Walker, T. D. Veal, C. F. McConville, H. Lu, and W. J. Schaff, Phys. Status Solidi C **2**, 2301 (2005).
[9]J. F. Moulder, W. F. Stickle, P. E. Sobol, and K. D. Bomben, *Handbook of X-Ray Photoelectron Spectroscopy* (Perkin-Elmer, Eden Prairie, 1992).
[10]T. D. Veal, I. Mahboob, L. F. J. Piper, T. Ashley, M. Hopkinson, and C. F. McConville, J. Phys.: Condens. Matter **16**, S3201 (2004).
[11]W. H. Gries, Surf. Interface Anal. **24**, 38 (1996).
[12]Y. Nanishi, Y. Saito, T. Yamaguchi, M. Hori, F. Matsuda, T. Araki, A. Suzuki, and T. Miyajima, Phys. Status Solidi A **200**, 202 (2003).
[13]A. R. Smith, R. M. Feenstra, D. W. Greve, M. S. Shin, M. Skowronski, J. Neugebauer, and J. E. Northrup, J. Vac. Sci. Technol. B **16**, 2242 (1998).
[14]J. E. Northrup, J. Neugebauer, R. M. Feenstra, and A. R. Smith, Phys. Rev. B **61**, 9932 (2000).
[15]H. Ibach and D. L. Mills, *Electron Energy Loss Spectroscopy and Surface Vibrations* (Academic, New York, 1982).
[16]I. Mahboob, T. D. Veal, C. F. McConville, H. Lu, and W. J. Schaff, Phys. Rev. Lett. **92**, 036804 (2004).
[17]L. F. J. Piper, T. D. Veal, I. Mahboob, C. F. McConville, H. Lu, and W. J. Schaff, Phys. Rev. B **70**, 115333 (2004).